Neuropsychologia 225 (2026) 109416

Contents lists available at ScienceDirect

Neuropsychologia

journal homepage: www.elsevier.com/locate/neuropsychologia

Patterns of functional connectivity differentiate individuals and individual regions in face and scene selective networks

David M. Watson [a,*], Kira N. Noad [a,b], Bartholomew P.A. Quinn [a,c], Timothy J. Andrews [a]

[a] Department of Psychology & York Neuroimaging Centre, University of York, York, UK
[b] Mathematisches Institut, Justus-Liebig-Universität Gießen, Gießen, Germany
[c] Institute of Cognitive Neuroscience, University College London, London, UK

ARTICLE INFO

Keywords:
Connectivity fingerprints
Functional connectivity
fMRI
Face perception
Scene perception

ABSTRACT

The perception and recognition of faces and scenes rely on distributed neural systems comprising specialised, category-selective regions in visual cortex that interact with an extended network of cortical regions across the brain. While prior work has demonstrated face- and scene-selective responses can be differentiated based on patterns of whole-brain connectivity, it remains unclear whether category-selective regions within each network also possess distinguishable whole-brain connectivity profiles reflecting their specific functional roles. It is also unclear whether individuals have distinct connectivity profiles that might underlie individual differences in face or scene perception. In this study, we used functional magnetic resonance imaging (fMRI) from multiple different naturalistic movie watching paradigms and at rest. We identified whole-brain functional connectivity fingerprints for each of the core regions within the face and scene processing networks. We found that patterns of functional connectivity were more similar within than between participants and were distinct across individual regions of the face and scene networks. These findings demonstrate that brain regions within category-selective visual networks are characterised by distinctive connectivity profiles with the rest of the brain.

1. Introduction

The perception of faces and scenes is supported by high-level visual regions located in occipital and posterior temporal cortices (Bracci and Op de Beeck, 2023; Peelen and Downing, 2017). Dedicated cortical networks have been identified within these brain regions that selectively process faces or scenes. The face-selective network includes a core set of regions in the ventral visual stream—the occipital face area (OFA), fusiform face area (FFA), and superior temporal sulcus (STS)—which together support the analysis of both invariant and dynamic facial features (Duchaine and Yovel, 2015; Haxby et al., 2000). In parallel, scene perception engages a core network comprising the occipital place area (OPA), parahippocampal place area (PPA), and retrosplenial complex (RSC), which are differentially involved in visuospatial and mnemonic processing (Baldassano et al., 2016; Epstein and Baker, 2019). These core face and place regions further interact with extended networks of regions throughout the parietal, frontal, and medial temporal lobes that are implicated in higher-level cognitive processing of people and places (Duchaine and Yovel, 2015; Epstein and Baker, 2019; Silson et al., 2019).

While the functional selectivity of these category-selective regions has been well characterized, an emerging view suggests that brain function is also influenced by broader patterns of connectivity with the rest of the brain (Mars et al., 2018; Passingham et al., 2002). It has been shown that the spatial location of category-selective regions can be predicted from whole-brain connectivity patterns (Molloy et al., 2024; Osher et al., 2016; Saygin et al., 2012). The importance of these connectivity profiles for brain development is shown by the fact they are present even before the emergence of category-specific responses (Kubota et al., 2025; Saygin et al., 2016). Despite these findings, it remains unclear whether individual regions within a given category-selective network can be distinguished from one another based solely on their functional connectivity profiles. That is, do connectivity profiles reveal a finer-grained organisation reflecting the distinct computational roles of regions within these networks?

A range of evidence demonstrates substantial and quantifiable individual differences in visual perception. For example, face recognition ability varies dramatically across the population, from people with developmental prosopagnosia to those who are 'super-recognizers' (Duchaine and Nakayama, 2006; Russell et al., 2009; White and Burton,

* Corresponding author.
E-mail address: david.watson@york.ac.uk (D.M. Watson).

https://doi.org/10.1016/j.neuropsychologia.2026.109416
Received 24 November 2025; Received in revised form 28 January 2026; Accepted 26 February 2026
Available online 27 February 2026

2022). Parallel work in scene perception shows similar variability across individuals (Clark and Maguire, 2023; Wang et al., 2024). Patterns of whole-brain connectivity have been shown to vary systematically across individuals (Finn et al., 2015; Shen et al., 2017). Such patterns have been referred to as "connectivity fingerprints", which are capable of identifying individuals within a large group. Connectivity fingerprints are also predictive of human behaviour and cognition, underscoring their relevance to brain function (Beaty et al., 2018; Rosenberg et al., 2016). Nevertheless, previous research has focussed on connectivity fingerprints measured on a global scale across the whole brain. It therefore remains unclear to what extent the connectivity profiles of the face and scene processing networks specifically are idiosyncratic.

In the present study, we examine patterns of functional connectivity among core regions of the face and scene networks during naturalistic movie viewing (Finn, 2021) and resting-state (Raichle, 2015) conditions. Specifically, we ask: (1) Are connectivity profiles of the face and scene networks idiosyncratic within individuals? (2) Do individual regions within these networks exhibit distinct and dissociable connectivity profiles? (3) To what extent are connectivity patterns of these networks modulated by task context or stimulus content? By probing these questions, we aim to advance our understanding of the functional architecture and network-level organisation of high-level visual cortex.

2. Methods

Details of the datasets and pre-processing pipelines reported here have been adapted from Watson and Andrews (2024). In all statistical tests we employ an $\alpha = .05$ criterion for statistical significance. Effect sizes for paired-samples tests are reported in units of Cohen's d_{av}, in which the mean of the pairwise differences is divided by the mean of the standard deviations of the two measures (Lakens, 2013).

2.1. Datasets

We obtained MRI data from three datasets – one dataset collected "in-house" (Game of Thrones) plus two further publicly available MRI datasets (StudyForrest and the Human Connectome Project).

2.1.1. Game of Thrones

This dataset was collected "in-house" and has been described previously in Noad et al. (2024). The dataset is publicly available on OpenNeuro (https://openneuro.org/datasets/ds004848). We tested 45 neurologically healthy participants with normal or corrected-to-normal vision (15 male, 30 female, age range = 18-32, median age = 19). Written consent was obtained from all participants, and the study was approved by the ethics committee of the York Neuroimaging Centre at the University of York (ethics code: P1442).

MRI data were collected at the York Neuroimaging Centre on a 3T Siemens Magnetom Prisma scanner using a 64-channel head coil. Functional data were acquired from 60 axial slices using a multiband EPI sequence (TR = 2 s, TE = 30 ms, FOV = 240 × 240 mm, matrix size = 80 × 80, 3 mm^3 isotropic voxels, flip angle = 80°, anterior-posterior phase encoding direction, multiband acceleration factor = 2). Additional field-map images were acquired in the same plane as the functional images (TR = 554 ms, short TE = 4.9 ms, long TE = 7.38 ms, flip angle = 60°, other parameters as per functional images). Finally, high-resolution T1-weighted anatomical images were acquired from 176 sagittal slices (TR = 2.3 s, TE = 2.26 ms, FOV = 256 × 256 mm, matrix size = 256 × 256, 1 mm^3 isotropic voxels, flip angle = 8°).

Participants completed two functional scans. In the first scan, participants passively viewed a naturalistic movie containing short audio-visual clips (lasting between 50 and 117 s; total duration = 12 min 58 s) taken from the *Game of Thrones* television series. Videos were presented at the full resolution of the screen (1920 × 1080 pixels, subtending approximately 38.7° × 22.3° visual angle). The second scan was a category localiser including images of faces, scenes, and phase scrambled faces, presented in a block design. Each block comprised 4 images from a given condition, presented sequentially (600 ms duration, 200 ms ISI) followed by a 6 s blank period. A mid-grey screen was displayed during the ISIs and blank periods. Nine blocks were included for each condition (27 blocks total, 4 min 4 s scan duration). Participants performed an orthogonal task detecting occasional changes in the colour of the fixation cross (responding via a button press) to maintain attention. Face images were obtained from the Radboud face database (Langner et al., 2010) and displayed on a grayscale pink noise background. Scene images were obtained from the SUN database (Xiao et al., 2010). All images subtended 8.4° degrees of visual angle. Stimuli were back-projected onto an in-bore screen at a viewing distance of approximately 57 cm. Stimuli were presented in PsychoPy v3.1.5 (Peirce et al., 2019).

2.1.2. StudyForrest

Movie-watching and functional localiser data for 15 participants were obtained from the StudyForrest MRI dataset (Hanke et al., 2014, 2016; Sengupta et al., 2016; https://www.studyforrest.org). In brief, the movie-watching paradigm comprised passive viewing of approximately 2 h of audiovisual clips from the *Forrest Gump* movie. The functional localiser included images of human bodies, human faces, houses, inanimate objects, scenes, and phase scrambled versions of those images, all presented within a block design. High-resolution T1-and T2-weighted anatomical images were also acquired. All data were acquired on a 3T Philips Achieva MRI scanner. Full details are provided in (Hanke et al., 2016; Sengupta et al., 2016).

2.1.3. Human Connectome Project

Movie-watching, resting-state, and task fMRI data were obtained from the Human Connectome Project (HCP; Van Essen, Ugurbil, et al., 2012). We employed a subset of 174 participants from the S1200 release who fully completed all resting-state and movie-watching scans. Three participants had missing task data and were omitted from functional localiser analyses (leaving $n = 171$). A list of the participants is provided in Supplementary Table 1.

Resting-state and movie-watching data were acquired on a 7T Siemens Magnetom MRI scanner. The movie-watching data included four scan runs (lasting between 11 and 14 min) during which participants passively viewed audiovisual clips taken from independent and Hollywood movies (Cutting et al., 2012). The resting-state data included four scan runs (each lasting approximately 16 min) in which participants viewed a fixation cross on a blank background with their eyes open.

Task fMRI data were acquired on a 3T Siemens Skyra MRI scanner with a customised gradient coil. We used data from the working memory task for the purposes of localising face- and scene-selective brain regions. Participants viewed images of human bodies, human faces, scenes, and tools while performing a 0-back or 2-back recognition task. Full details of all HCP datasets can be found in the WU-Minn HCP S1200 Data Release reference manual.

2.2. Pre-processing

2.2.1. Game of Thrones and StudyForrest

Both the Game of Thrones and StudyForrest datasets were pre-processed using FSL (Jenkinson et al., 2012). Initial pre-processing was performed in FEAT. Pre-processing of the localiser data included the following steps: motion correction using MCFLIRT (Jenkinson et al., 2002), slice-timing correction, non-brain removal using BET (Smith, 2002), spatial smoothing using a Gaussian kernel (FWHM = 6 mm, twice the voxel size), grand-mean intensity normalisation by a single multiplicative factor, and high-pass temporal filtering. Filter bandwidths were set at $\sigma = 25$ s and $\sigma = 24$ s for the Game of Thrones and StudyForrest localiser datasets respectively.

Pre-processing of the movie-watching data followed the same pipeline as the localiser data, but included two additional denoising steps

intended to mitigate the effects of head motion. Firstly, an ICA-based denoising strategy was applied prior to the temporal filtering but following all other pre-processing steps. MELODIC (Beckmann and Smith, 2004) estimated spatiotemporal independent components from the data, then ICA-AROMA (Pruim et al., 2015) identified noise components associated with head motion and regressed them out of the data. We used an aggressive denoising strategy, whereby all variance associated with noise components was removed. High-pass temporal filtering ($\sigma = 50$ s) was applied after the ICA denoising. Secondly, a component-based (CompCor) denoising strategy (Behzadi et al., 2007) was applied to remove CSF-related components. Tissue segmentations were derived from the high resolution anatomical images (T1-weighted for Game of Thrones, and T1-and T2-weighted for StudyForrest) using FSL's FAST tool (Zhang et al., 2001). A mask of CSF voxels was generated by transforming the partial volume estimates to the functional volumes then thresholding at 90% and binarising. The mean and first 4 principal component timeseries from the CSF voxels were then regressed out of the functional data.

FSL's BET tool was used to remove non-brain material from the high-resolution T1 anatomical images. Functional images were then co-registered to the T1 anatomical images via boundary-based registration (Greve and Fischl, 2009). For the Games of Thrones dataset, field-maps were used to additionally apply B0 unwarping to the functional images. Anatomical images were then registered to the MNI152 brain via a nonlinear registration using FNIRT (Andersson et al., 2010).

2.2.2. Human Connectome Project

The HCP data were obtained following application of the HCP minimal pre-processing pipeline (Glasser et al., 2013; Smith et al., 2013) including ICA-based denoising. Briefly, this includes gradient distortion correction, motion correction, high-pass temporal filtering ($\sigma = 1000$ s), and automated removal of noise components via FSL's FIX tool (Salimi-Khorshidi et al., 2014). Cortical data were registered to the fsLR32k standard surface (Van Essen, Glasser, et al., 2012) via a multimodal surface-based alignment (MSMAll; Robinson et al., 2014; 2018) which incorporates information about cortical folding, resting-state network and visuo-topic maps, and areal features derived from myelin maps. We applied additional surface-based spatial smoothing on top of that performed in the minimal pipeline to achieve an effective FWHM of 3.2 mm for resting-state and movie-watching data, and 4 mm for task data (twice the voxel resolution). For the task data, we additionally applied a more stringent high pass temporal filter ($\sigma = 100$ s).

2.3. Regions of interest

2.3.1. Face and scene-selective regions

We functionally defined group-level regions of interest (ROIs) for the core face-selective (Occipital Face Area [OFA], Fusiform Face Area [FFA], Superior Temporal Sulcus [STS]) and scene-selective regions (Occipital Place Area [OPA], Parahippocampal Place Area [PPA], Retrosplenial Complex [RSC]). Supplementary Fig. 1 shows the locations of the face- and scene-selective ROIs in each dataset. A summary of the location and size of each ROI is provided in Supplementary Table 2.

We analysed the Game of Thrones and StudyForrest data using FEAT. Boxcar regressors for each condition (Game of Thrones: faces, scenes, and scrambled faces; StudyForrest: bodies, faces, houses, objects, scenes, and scrambled) were convolved with a single-gamma hemodynamic response function. These regressors were entered a first-level GLM analysis (Woolrich et al., 2001) alongside their temporal derivatives and six head motion confound regressors. Face-selective contrasts were defined as "faces > (scenes + scrambled faces)" for Game of Thrones and "faces > (scenes + houses)" for StudyForrest. Conversely, scene-selective contrasts were defined as "scenes > (faces + scrambled faces)" for the Game of Thrones and "(scenes + houses) > faces" for StudyForrest. For the StudyForrest dataset only, first-level parameter estimates were averaged over scan runs by higher-level fixed effects analyses (Woolrich et al., 2004). Individual estimates were then combined over subjects by a higher-level mixed-effects analysis using FLAME. ROIs were defined using a custom clustering algorithm applied to the face- and scene-selective statistical maps. Peak voxels within each of the target regions were defined as seeds, and the algorithm iteratively adjusted the statistical threshold to derive clusters of 250 spatially contiguous voxels (2000 mm^3) around the seeds. Actual cluster sizes varied slightly as an optimal solution was not always possible. Finally, group level ROIs were transformed from the MNI volume to each participant's functional volume.

We analysed the HCP task data using scripts from the HCP analysis pipelines (https://github.com/Washington-University/HCPpipelines; Glasser et al., 2013), which internally use FEAT. In the working memory task, participants perform a 0-back or 2-back recognition task on images from different visual object categories. Category selective regions can be localised from these data by contrasting the object categories while collapsing over the recognition tasks (Barch et al., 2013). Eight boxcar regressors for each condition (bodies, faces, scenes, and tools in each task) were convolved with a double-gamma hemodynamic response function. These regressors were entered into a first-level GLM analysis alongside their temporal derivatives plus twelve confound regressors comprising head motion parameters and their temporal derivatives. Face-selective responses were localised by the contrast of "faces > scenes", and scene-selective responses by the reverse contrast. Parameter estimates were averaged over scan runs within each participant by higher-level fixed-effects analyses, and then further over participants by a higher-level mixed-effects analysis using FLAME. ROIs were defined on the cortical surface using a custom clustering algorithm to derive 500 mm^2 clusters of spatially contiguous vertices around the peak vertices for each face and scene region.

2.3.2. Cortical parcellation

We also obtained a whole-brain parcellation from the Schaefer atlas, which divides the cortex into a series of functionally distinct parcels based on resting-state functional connectivity (Schaefer et al., 2018). We used the 200-area version of this parcellation (100 parcels in each hemisphere) as this has previously been shown to maximise functional differences between parcels (Zhi et al., 2022). For the Game of Thrones and StudyForrest datasets, cortical surfaces for each subject were reconstructed from their anatomical scans using Freesurfer (Dale et al., 1999). The parcellation was transformed from the *fsaverage* surface to each subject's native surface, and then further projected back into their functional volumes. For the HCP datasets, we used the parcellation as provided on the fsLR32k surface.

2.4. Functional connectivity analyses

2.4.1. Measuring split-half connectivity

Connectivity analyses were performed in the native functional volumes for the Game of Thrones and StudyForrest datasets, and in the fsLR32k standard space for the HCP datasets. The pre-processed and denoised functional timeseries from the movie-watching and resting-state scans were converted to units of percent signal change. The timeseries were then divided into two independent splits of each dataset. For the Game of Thrones dataset, which contains only a single scan run, timeseries were split between the first and second halves of the scan run. For the StudyForrest and HCP datasets, timeseries were concatenated over odd and even scan runs separately. Timeseries were then averaged over grayordinates within each of the face and scene regions and the 200 Schaefer parcels. For each data split independently, functional connectivity was measured by correlating the averaged timeseries of each face and scene region with the averaged timeseries for each parcel. This produced a series of correlation/connectivity matrices for each subject and data split, with 6 face or scene regions (across both hemispheres) represented in the rows and 200 parcels (across both hemispheres) represented in the columns. All correlations were converted to units of

Fisher's z prior to further analysis.

2.4.2. Comparing fingerprints between subjects

We tested the ability to individuate subjects using the split-half connectivity fingerprints of the face and scene networks. For each subject, their connectivity matrices (between the 6 face/scene regions and 200 Schaefer parcels) were correlated across the data splits both with their own matrix from the other data split (within-subject comparison) and with the matrices from each of the other subjects in the same dataset (between-subject comparisons).

We performed two analyses to individuate subjects. We first conducted a parametric analysis. For each subject, the between-subject correlations were averaged over the other subjects and data splits, such that each subject was allocated a within-subject correlation and an average between-subject correlation. We then used paired-samples t-tests to contrast the within-subject versus average between-subject correlations across subjects.

Secondly, we performed classification analyses, applying two alternative classification strategies. We conducted a pairwise classification analysis that compared each pair of subjects in turn. For a given subject, we compared their within-subject correlation against their between-subject correlations with each of the other subjects in turn. For each comparison, the subject was considered correctly classified if their within-subject correlation was higher than the between-subject correlation. This produced a total of $2(N-1)$ binary values (one for each data split and between-subject comparison), which were averaged together to produce an overall proportion decoding accuracy for that subject. We also repeated this analysis using a one-versus-rest classification strategy, in which a subject was only considered correctly classified if their within-subject correlation was higher than *all* their correlations with the other subjects. For each subject, this produced two binary values (one per data split) which were averaged together. Thus, the expected chance level is 50% accuracy under the pairwise strategy, and $100/N$ percent accuracy in the one-versus-rest strategy. For both strategies, statistical significance was assessed using permutation testing. The order of subjects was randomly shuffled in each data split independently, then decoding accuracies were calculated as described above and averaged over subjects. This was repeated for 10,000 permutations to derive an empirical null distribution (including the "true" permutation, without shuffling the subjects). Statistical significance was defined by the proportion of values in the null distribution greater than or equal to the true group average accuracy.

In assessing statistical significance for both the parametric and classification analyses, a Holm-Bonferroni correction for multiple comparisons (Holm, 1979) was applied over the face/scene networks and the 4 datasets (8 comparisons).

2.4.3. Comparing region-level fingerprints

We next adapted our approach to compare split-half connectivity fingerprints for individual regions within the face and scene networks separately. Each row of the connectivity matrices represents a *region-level* connectivity fingerprint, measuring the pattern of connectivity between a specific face or scene region with each of 200 Schaefer parcels. We tested the ability to decode individual regions from these region-level connectivity fingerprints. For each subject and region, we correlated the region-level connectivity fingerprints across the data splits. This produced a 6×6 asymmetrical matrix of second-order correlations (comprising 6 within-region and 30 between-region comparisons) for each subject. Note that for simplicity, we only considered within-subject comparisons for this analysis.

We applied both parametric and classification analyses to decode the face and scene regions. In the parametric analysis, the correlations were averaged over each of the within-region and between-region comparisons separately, such that each subject was allocated an average within-region and an average between-region correlation. We then used paired-samples t-tests to contrast the within-versus between-region correlations across subjects.

Next, we again performed classification analyses using both pairwise and one-versus-rest strategies. In the pairwise approach, for each subject and region we compared the within-region correlation against the between-region correlations with each of the other regions in turn. For each comparison, the region was considered correctly classified if the within-region correlation was higher than the between-region correlation. This produced a total of 60 binary values (one for each of the 30 region pairings and data splits), which were averaged together to produce an overall proportion decoding accuracy for that subject. With the one-versus-rest strategy, a region was only considered correctly classified if its within-region correlation was higher than *all* of its correlations with the other regions. This produced 12 binary values (one for each of the 6 regions and data splits), which were averaged together to yield an overall proportion decoding accuracy for that subject. Thus, the expected chance level is 50% accuracy under the pairwise strategy, and $[100/6 = 16.67\%]$ for the one-versus-rest strategy. Again, statistical significance was assessed using permutation testing – the order of regions was randomly shuffled in each data split independently (applying the same random ordering across subjects), then decoding accuracies were calculated as described above and averaged over subjects. This was repeated for 10,000 permutations to derive an empirical null distribution (including the "true" permutation, without shuffling the regions). Statistical significance was defined by the proportion of values in the null distribution greater than or equal to the true group average accuracy.

In assessing statistical significance for both the parametric and classification analyses, a Holm-Bonferroni correction for multiple comparisons (Holm, 1979) was applied over the face/scene networks and the 4 datasets (8 comparisons).

2.4.4. Comparing fingerprints between HCP tasks

Finally, we compared the connectivity fingerprints between subjects and within and between the movie-watching and rest-state tasks of the HCP dataset. For each subject, their connectivity matrices for each task were correlated across the data splits with the other subjects in both tasks. These correlations were then grouped into within-movie-watching, within-resting-state, and between-task comparisons, and averaged within each grouping. This yielded three averaged correlation values per subject.

We then conducted further parametric analyses to compare correlations across the task combinations. A two-way repeated-measures ANOVA was conducted with factors for the network (face, scene) and task-comparison (within-movie-watching, within-resting-state, between-task). Effect sizes are reported in units of partial and generalised eta squared (Bakeman, 2005; Olejnik and Algina, 2003). We also employed a series of post-hoc paired-samples t-tests contrasting each pairwise combination of task-comparisons for each network. A Holm-Bonferroni correction (Holm, 1979) was applied over the 3 pairwise combinations and face/scene networks (6 comparisons).

3. Results

We measured the functional connectivity of face- and scene-selective regions to 200 cortical parcels across the whole brain (Schaefer et al., 2018) in three movie-watching datasets (Game of Thrones, StudyForrest, and HCP – Movie) and one resting-state dataset (HCP – Rest). Importantly, face- and scene-selective regions were defined from independent task-based functional localisers specific to each dataset. Connectivity was estimated in two independent splits of each dataset.

The Schaefer parcels can be labelled according to their overlap with 17 resting-state networks in the Yeo atlas (Yeo et al., 2011). To visualise the connectivity fingerprints for each region, we averaged the connectivity values over subjects and over parcels within each of these 17 networks (Fig. 1). Connectivity patterns within each network were similar across datasets and between splits within each dataset. Within

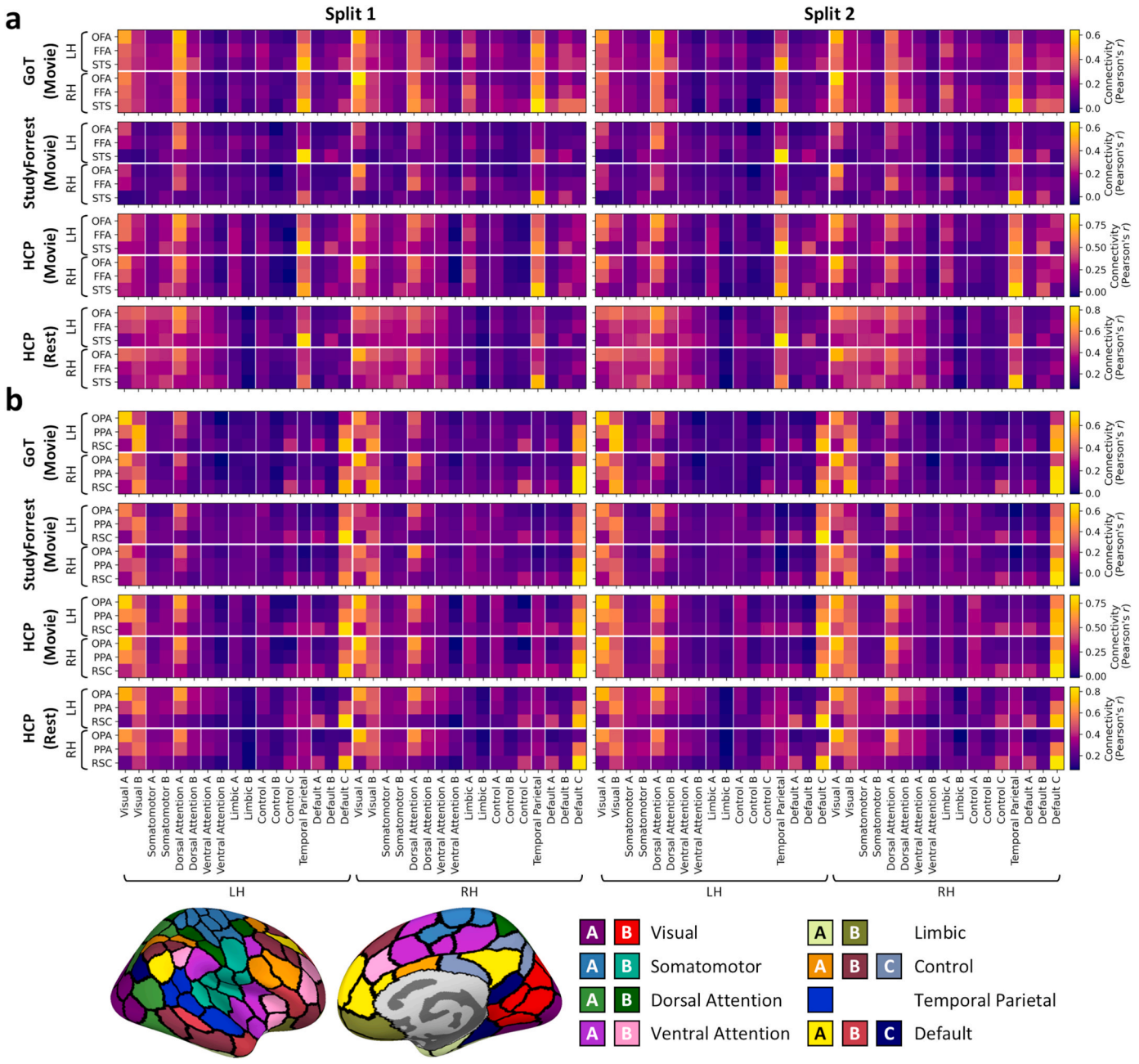

Fig. 1. Functional connectivity fingerprints of (a) face and (b) scene-selective regions with the 200-area Schaefer parcellation of the cortex (Schaefer et al., 2018), averaged over subjects and over parcels in each of 17 resting-state networks (Yeo et al., 2011). Connectivity was estimated separately for two independent splits of each of the Game of Thrones, StudyForrest, and HCP movie-watching and resting-state datasets. Locations of parcels, colour-coded by the 17 resting-state networks, are illustrated along the bottom. (For interpretation of the references to colour in this figure legend, the reader is referred to the Web version of this article.)

the face network, the OFA and FFA were preferentially connected with early visual and dorsal attention networks. In contrast, the STS showed stronger connectivity with the temporoparietal and default mode networks. Meanwhile, within the scene network, the OPA was preferentially connected with early visual and dorsal attention networks, while the RSC was more strongly connected with anterior visual, frontoparietal control, and default mode networks.

3.1. *Individuating subjects*

We correlated the connectivity fingerprints across the data splits within- and between-subjects in each dataset. Fig. 2a illustrates the distributions of fingerprint similarities over subjects for within- and between-subject comparisons. In all cases, positive correlations were observed between connectivity fingerprints for both within- and between-subject comparisons. Nevertheless, a series of paired-samples t-tests (Table 1) indicated that fingerprints were significantly more similar within than between-subjects (all $p < .001$). Notably, the high within-subject correlations also demonstrate high split-half reliability of the connectivity fingerprints.

We also applied a classification analysis to individuate subjects from the connectivity fingerprints. Using a pairwise decoding strategy, we compared each subject's within-subject correlation against their between-subject correlation with each other subject in turn. A comparison was considered correctly classified if the within-subject correlation was higher than the between-subject correlation. The accuracies were then averaged over comparisons within each subject. Fig. 2b illustrates the mean and confidence intervals of these accuracies over

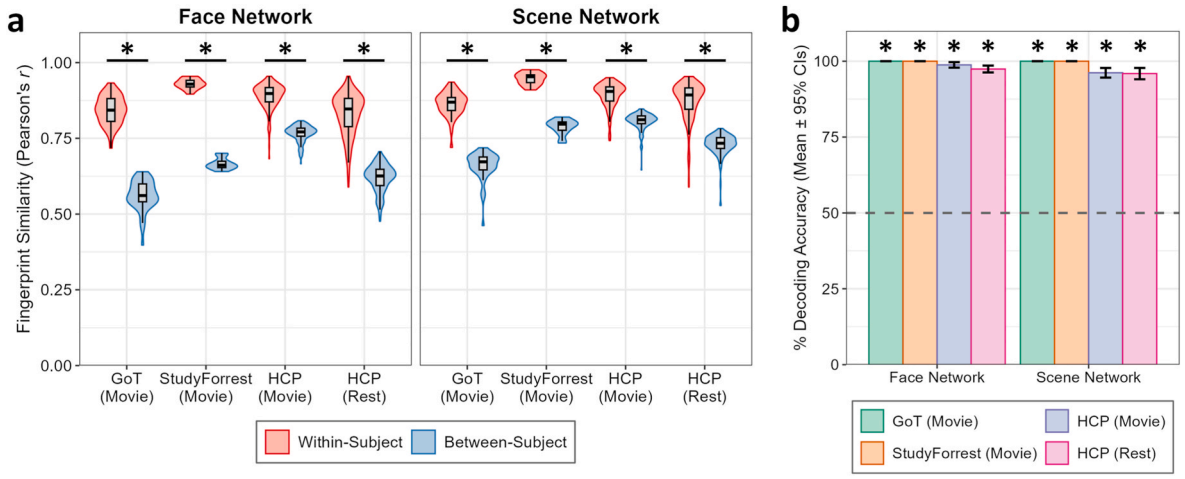

Fig. 2. Individuation of subjects by connectivity fingerprints of face and scene networks. Connectivity fingerprints were correlated within and between subjects across the data splits. (a) Violin plots illustrate distributions of within-subject and average between-subject correlations over subjects. Asterisks denote significant within versus between-subject correlation differences as determined by paired-samples t-tests (all $p < .001$). (b) Decoding accuracy using pairwise classification strategy. For each subject, an overall accuracy is calculated over a series of classifications testing if their within-subject correlation is higher than their correlation with each other subject in turn. Bars illustrate means and 95% confidence intervals over subjects. Asterisks denote significant decoding accuracies determined by permutation testing (all $p < .001$). The dashed line indicates the expected chance level.

Table 1
Paired-samples t-tests contrasting within-subject > between-subject connectivity fingerprint correlations.

Network	Dataset	Cohen's d_{av}	t	DoF	p
Face	GoT	5.22	29.79	44	<.001
	StudyForrest	11.18	30.02	14	<.001
	HCP (Movie)	3.57	38.14	173	<.001
	HCP (Rest)	3.42	31.99	173	<.001
Scene	GoT	4.63	31.77	44	<.001
	StudyForrest	5.83	17.82	14	<.001
	HCP (Movie)	2.73	30.10	173	<.001
	HCP (Rest)	3.09	28.35	173	<.001

subjects. Classification accuracies appeared close to ceiling performance, and permutation tests confirmed that all accuracies were significantly above chance performance (all $p < .001$; Supplementary Fig. 2a). For a stricter test of classification performance, we also employed a one-versus-rest decoding strategy in which a given subject would only be correctly classified if their within-subject correlation was higher than *all* their between-subject correlations (Supplementary Fig. 3a). While classification accuracies were often lower than when using the pairwise decoding strategy – especially in the larger HCP dataset – they all remained significantly above chance performance (all $p < .001$; Supplementary Fig. 2b).

Thus, while connectivity fingerprints of face and scene networks with the rest of the brain showed substantial commonalities across participants, they also included idiosyncrasies sufficient to reliably individuate subjects.

3.2. Decoding face and scene regions

Each row of the connectivity matrices provides a *region-level* connectivity fingerprint, representing the pattern of functional connectivity

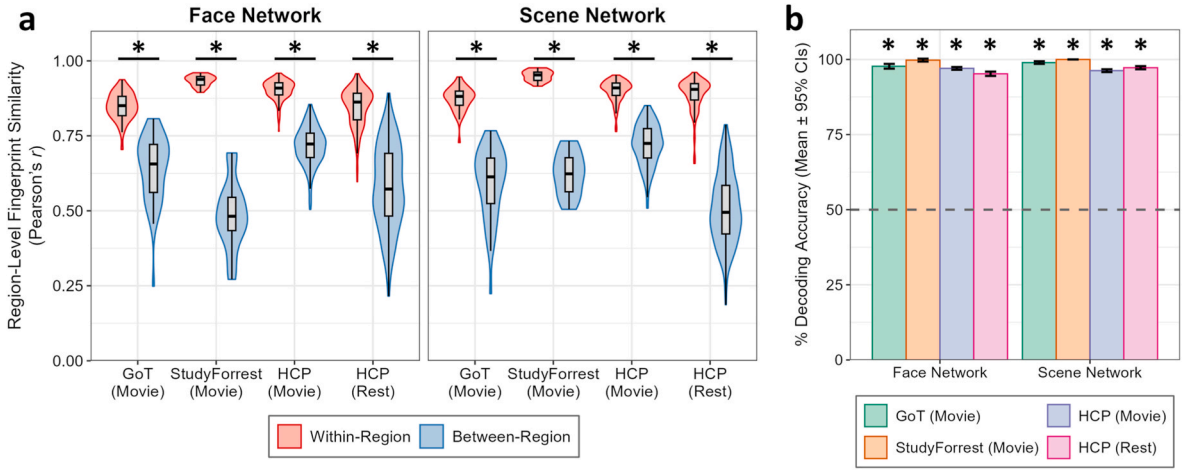

Fig. 3. Identifying regions within face and scene networks by region-level connectivity fingerprints. Connectivity fingerprints were correlated within and between regions in the face and scene networks. (a) Correlations were averaged over within and between-region pairings for each subject. Violin plots illustrate distributions of these correlations across subjects. Asterisks denote significant within versus between-region correlation differences as determined by paired-samples t-tests (all $p < .001$). (b) Decoding accuracy using pairwise classification strategy. For each subject, an overall accuracy is calculated over a series of classifications testing if each within-region correlation is higher than the correlation with each other region in turn. Bars illustrate means and 95% confidence intervals over subjects. Asterisks denote significant decoding accuracies determined by permutation testing (all $p < .01$). The dashed line indicates the expected chance level.

for a specific face or scene region with the cortical networks throughout the brain. We correlated these region-level fingerprints across the data splits within and between regions for each subject. Supplementary Fig. 4 shows matrices illustrating the group-average correlations between each pairing of regions. We averaged the fingerprint correlations over within-region and between-region pairings for each subject. Fig. 3a illustrates the distributions of these averaged correlations over subjects. A series of paired-samples t-tests (Table 2) confirmed that the within-region correlations were significantly higher than between-region correlations (all $p < .001$).

We next performed classification analyses of the region-level connectivity fingerprints. We first adopted a pairwise decoding strategy, comparing the within-region correlation for each region against its between-region correlations with each other region in turn. A comparison was considered correctly classified if the within-region correlation was higher than the between-region correlation. These accuracies were then averaged over all region pairings within each subject. Fig. 3b illustrates the means and confidence intervals of the accuracies over subjects. The accuracies appeared close to ceiling performance, and permutation tests confirmed that they were all significantly above chance performance (all $p < .01$; Supplementary Fig. 2c). A stricter test of classification performance was also obtained using a one-versus-rest strategy, in which a region was only considered correctly classified if its within-region correlation was higher than *all* its between-region correlations (Supplementary Fig. 3b). Classification accuracies were lower than with the pairwise strategy but nevertheless remained significantly above chance (all $p < .05$; Supplementary Fig. 2d).

Thus, the connectivity fingerprints of the face and scene regions with the rest of the brain were regionally specific, sufficient to reliably differentiate regions within each network.

3.3. Comparing HCP tasks

Finally, we compared connectivity fingerprints across the movie-watching and resting-state tasks between subjects in the HCP dataset. Critically, each of these tasks comprise the same subjects, were acquired with the same scan parameters, and use the same preprocessing pipeline and ROI definitions – they differ only in terms of the task itself. For each HCP subject and task, we correlated their connectivity fingerprints across the data splits with other subjects' fingerprints for both tasks. These correlations were then averaged for within-movie-watching, within-resting-state, and between-task comparisons in each subject. Note that the within-task comparisons here are equivalent to the between-subject comparisons presented in the analyses of individual differences (cf. Fig. 2a).

Fig. 4 shows the distributions of within-movie-watching, within-resting-state, and between-task correlations over subjects. For both the face and scene networks, strong positive correlations were observed in all task comparisons, indicating clear commonalities in connectivity fingerprints derived from movie-watching and resting-state. Nevertheless, the connectivity fingerprints also appeared more similar for within- than between-task comparisons, thereby also showing task-specific contributions. A repeated-measures ANOVA revealed a significant main effect of network ($F(1, 173) = 1835.78$, $p < .001$, $\eta_P^2 = .91$, $\eta_G^2 = .62$) due to overall higher correlations for the scene network. There was also a significant main effect of task-comparison ($F(1.85, 320.41) = 2664.23$, $p < .001$, $\eta_P^2 = .94$, $\eta_G^2 = .65$); a series of paired-samples t-tests revealed correlations were significantly higher for the within-movie-watching comparisons, followed by within-resting-state comparisons, then between-task comparisons (all $p < .001$; Table 3). There was also a significant task-comparison by network interaction ($F(1.69, 292.29) = 206.59$, $p < .001$, $\eta_P^2 = .54$, $\eta_G^2 = .04$) because the differences between task-comparisons were larger for the face than scene network.

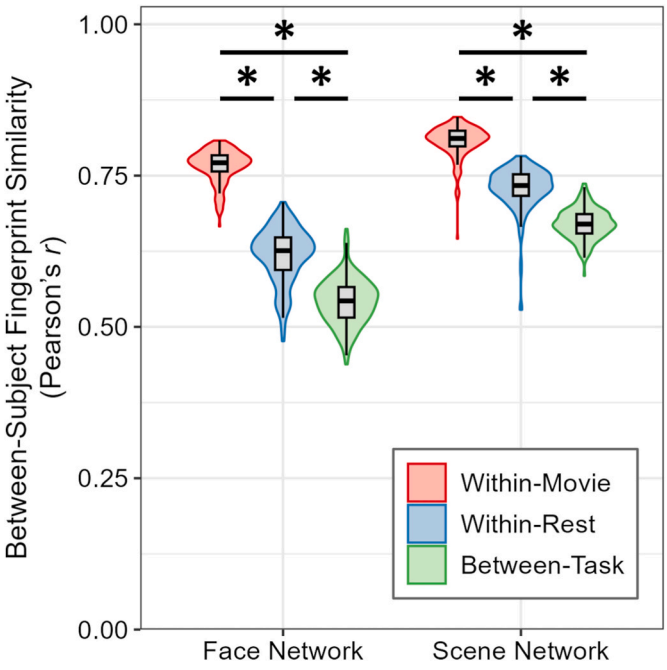

Fig. 4. Between-subject correlations of connectivity fingerprints within and between tasks in the HCP dataset. For each subject and task, connectivity fingerprints were correlated with other subjects in both tasks, then averaged for within-movie-watching, within-rest-state, and between-task comparisons. Violin plots illustrate the distributions of these averaged correlations over subjects. The different task-comparisons were contrasted against each other using paired-samples t-tests – asterisks indicate significant differences (all $p < .001$).

To further test how connectivity fingerprints generalise across tasks, we repeated our previous analyses individuating subjects and decoding face/scene regions, only now correlating the connectivity fingerprints *between* the HCP tasks (Supplementary Fig. 5). Although decoding performance was reduced relative to the within-task analyses (cf. Figs. 2 and 3, Supplementary Fig. 3), it nevertheless remained highly significant.

Thus, the connectivity fingerprints of the face and scene regions were consistent between subjects, and across movie-watching and resting-

Table 2
Paired-samples t-tests of region-level connectivity fingerprint correlations, contrasting within-region > between-region.

Network	Dataset	Cohen's d_{av}	t	DoF	p
Face	GoT	2.85	31.66	44	<.001
	StudyForrest	7.99	24.17	14	<.001
	HCP (Movie)	4.05	60.96	173	<.001
	HCP (Rest)	2.67	37.66	173	<.001
Scene	GoT	3.98	34.56	44	<.001
	StudyForrest	7.39	26.59	14	<.001
	HCP (Movie)	3.65	62.42	173	<.001
	HCP (Rest)	4.53	44.23	173	<.001

Table 3
Paired-samples t-tests contrasting between-subject correlations of connectivity fingerprints in the HCP dataset across the different task comparisons.

Network	Contrast	Cohen's d_{av}	t	DoF	p
Face	Within-Movie > Within-Rest	4.28	46.67	173	<.001
	Within-Movie > Between-Task	6.97	72.96	173	<.001
	Within-Rest > Between-Task	1.89	21.76	173	<.001
Scene	Within-Movie > Within-Rest	2.70	29.02	173	<.001
	Within-Movie > Between-Task	5.30	56.03	173	<.001
	Within-Rest > Between-Task	2.01	25.19	173	<.001

state tasks, but also included task-specific variation. Fingerprints were more similar for within-task than between-task comparisons – especially within the movie-watching task. Furthermore, patterns in the connectivity fingerprints, which identify individual subjects and brain regions, also generalised across the tasks.

4. Discussion

In this study, we analysed multiple fMRI datasets, including both movie-watching and resting-state paradigms, to characterise the functional connectivity profiles of core face- and scene-selective cortical regions across the brain. Connectivity fingerprints were highly reproducible across independent data splits and were more similar within than between individuals, highlighting their idiosyncratic nature. Region-level fingerprints also reliably distinguished individual regions within each network. Furthermore, while core features of the fingerprints were preserved across movie-watching and resting-state tasks, they also exhibited systematic variations as a function of task.

The distinct patterns of connectivity between face- and scene-selective regions and the rest of the brain provide distinct "fingerprints" for each network. While connectivity profiles showed substantial similarity across participants, they were markedly more consistent within individuals. These idiosyncratic features align with previous demonstrations that whole-brain connectomes can reliably identify individuals and predict individual differences in cognition and behaviour (Beaty et al., 2018; Finn et al., 2015; Kröll et al., 2023; Rosenberg et al., 2016; Shen et al., 2017). Our approach complements these insights by showing that idiosyncratic connectivity extends to category-selective visual regions, suggesting that individual differences in face and scene perception may be reflected in these neural connectivity signatures.

We also found distinct region-level connectivity profiles, demonstrating that functional differences between regions within the face and scene networks are also reflected in distinct patterns of connectivity of each region with the rest of the brain. This accords with previous studies demonstrating that the connectivity profiles of voxels in the ventral stream are predictive of their anatomical locations and functional tunings to visual objects (Molloy et al., 2024; Osher et al., 2016; Saygin et al., 2012). More generally, these results underscore how the functional specialisations of brain regions are underpinned by their connectivity with wider networks across the brain (Passingham et al., 2002).

The connectivity patterns revealed in this study imply that higher-level aspects of face and scene processing depend on extended networks of regions throughout the brain. Recent studies have shown that regions in the medial parietal and anterior temporal cortices are involved in the recognition and mental imagery of familiar people and places (Silson et al., 2019; Steel et al., 2021). Meanwhile, posterior parietal cortices have been linked to processing egocentric motion through scenes (Kennedy et al., 2024; Yoon et al., 2025), and the medial temporal lobes are important for navigation and memory for places (Epstein and Baker, 2019). Similarly, regions in the anterior temporal lobes and prefrontal cortex have been implicated in higher-level processing of faces, such as representing personal identity or extracting social cues from faces (Duchaine and Yovel, 2015). Future research could investigate how the connectivity fingerprints of these extended regions track their functional specialisations and individual differences in behaviour. More generally, our methods could be extended to differentiate connectivity fingerprints between regions in many other networks throughout the brain beyond the face and scene processing networks.

The distinct connectivity profiles we show for different regions within the face network align with established models of functional specialization. The OFA and FFA displayed preferential connectivity with early visual and dorsal attention networks, while the STS was more strongly connected with temporoparietal and default mode networks. These findings converge with previous work demonstrating weaker connectivity between the STS and ventral face-selective regions (Davies-Thompson and Andrews, 2012; Gschwind et al., 2012; Pyles et al., 2013), supporting contemporary models proposing divisions between a ventral pathway processing invariant facial features and a dorsal pathway processing dynamic facial information (Bernstein and Yovel, 2015; Duchaine and Yovel, 2015; Pitcher and Ungerleider, 2021). Meanwhile, for scene-selective regions, our results reinforce a functional distinction between a posterior network (e.g., OPA) linked with early visual and dorsal parietal networks, and an anterior network (e.g., RSC) associated with frontoparietal control and default mode networks, with each network converging in the PPA (Baldassano et al., 2016; Watson and Andrews, 2024). This functional segregation is consistent with evidence suggesting that different regions contribute to distinct aspects of scene processing, including recognition (PPA), egocentric navigation (OPA), and allocentric navigation (RSC) (Dilks et al., 2022; Julian et al., 2018).

Abstracting our analyses to the level of connectivity fingerprints allowed us to compare connectivity even when the underlying neural fluctuations were unrelated, such as across independent data splits or across different movie-watching or resting-state tasks. We found that patterns of connectivity were consistent across the datasets despite differences in participant groups, acquisition parameters, preprocessing pipelines, use of both movie-watching and resting-state paradigms (including different movie content, and different durations of scans), and slight variations in ROI definitions from independent localisers unique to each dataset. This demonstrates the connectivity fingerprints were robust to many methodological differences that may vary between experiments.

Nevertheless, we also observed stimulus-specific variation between the movie-watching and resting-state tasks in the Human Connectome Project. Importantly, these tasks comprised identical participants, acquisition parameters, preprocessing pipelines, and ROI definitions, thereby allowing us to isolate the effects of task from other extraneous variables varying between the datasets. Connectivity fingerprints were generally more similar within than between tasks – especially in the case of movie-watching. These results align with prior studies reporting robust yet stimulus-sensitive patterns of whole-brain connectivity across naturalistic and resting-state conditions (Kim et al., 2018; Lynch et al., 2018). Furthermore, they underscore the benefit of naturalistic viewing paradigms for studying brain function and connectivity (Finn, 2021; Rajimehr et al., 2024). Together, these findings highlight that while functional connectivity fingerprints of the face and scene networks are robust, they are also influenced by the stimulus, underscoring the modulatory role of task context in the response of visual networks. Future research might also examine how connectivity fingerprints are modulated by attention and task demands (Baldauf and Desimone, 2014; Harel et al., 2014).

5. Conclusion

In summary, we demonstrate that face- and scene-selective cortical regions exhibit distinct, individualised, and context-sensitive functional connectivity fingerprints. These findings are consistent with the idea that the functional properties of individual brain regions are closely linked to their unique pattern of connections with the rest of the brain. Connectivity fingerprints reveal both the common architecture and individual variability that shape category-selective processing in the human brain. Our findings also underline the need to consider task and stimulus context when interpreting the functional responses of category-selective networks.

CRediT authorship contribution statement

David M. Watson: Writing – review & editing, Writing – original draft, Visualization, Methodology, Investigation, Formal analysis, Conceptualization. **Kira N. Noad:** Writing – review & editing, Writing –

original draft, Methodology, Investigation, Conceptualization. **Bartholomew P.A. Quinn:** Writing – review & editing, Writing – original draft, Methodology, Investigation, Conceptualization. **Timothy J. Andrews:** Writing – review & editing, Writing – original draft, Supervision, Methodology, Conceptualization.

Acknowledgements

Data were provided in part by the Human Connectome Project, WU-Minn Consortium (Principal Investigators: David Van Essen and Kamil Ugurbil; 1U54MH091657) funded by the 16 NIH Institutes and Centres that support the NIH Blueprint for Neuroscience Research; and by the McDonnell Centre for Systems Neuroscience at Washington University.

Appendix A. Supplementary data

Supplementary data to this article can be found online at https://doi.org/10.1016/j.neuropsychologia.2026.109416.

Data availability

MRI data for the Game of Thrones dataset is available on OpenNeuro (https://openneuro.org/datasets/ds004848). MRI data for the StudyForrest and HCP datasets were obtained from already publicly available repositories. The analysis code and data for the connectivity fingerprint analyses are available on the Open Science Framework (https://osf.io/93dva).

References

Andersson, J.L.R., Jenkinson, M., Smith, S., 2010. Non-Linear Registration, Aka Spatial Normalization (FMRIB Technical Report TR07JA2) (Issue June). FMRIB Centre, Oxford, United Kingdom.

Bakeman, R., 2005. Recommended effect size statistics for repeated measures designs. Behav. Res. Methods 37 (3), 379–384. https://doi.org/10.3758/BF03192707.

Baldassano, C., Esteva, A., Fei-Fei, L., Beck, D.M., 2016. Two distinct scene-processing networks connecting vision and memory. eNeuro 3 (5), 1–14. https://doi.org/10.1523/ENEURO.0178-16.2016.

Baldauf, D., Desimone, R., 2014. Neural mechanisms of object-based attention. Science 344 (6182), 424–427. https://doi.org/10.1126/science.1247003.

Barch, D.M., Burgess, G.C., Harms, M.P., Petersen, S.E., Schlaggar, B.L., Corbetta, M., Glasser, M.F., Curtiss, S., Dixit, S., Feldt, C., Nolan, D., Bryant, E., Hartley, T., Footer, O., Bjork, J.M., Poldrack, R., Smith, S., Johansen-Berg, H., Snyder, A.Z., Van Essen, D.C., 2013. Function in the human connectome: Task-fMRI and individual differences in behavior. Neuroimage 80, 169–189. https://doi.org/10.1016/j.neuroimage.2013.05.033.

Beaty, R.E., Kenett, Y.N., Christensen, A.P., Rosenberg, M.D., Benedek, M., Chen, Q., Fink, A., Qiu, J., Kwapil, T.R., Kane, M.J., Silvia, P.J., 2018. Robust prediction of individual creative ability from brain functional connectivity. Proc. Natl. Acad. Sci. 115 (5), 1087–1092. https://doi.org/10.1073/pnas.1713532115.

Beckmann, C.F., Smith, S.M., 2004. Probabilistic independent component analysis for functional magnetic resonance imaging. IEEE Trans. Med. Imag. 23 (2), 137–152. https://doi.org/10.1109/TMI.2003.822821.

Behzadi, Y., Restom, K., Liau, J., Liu, T.T., 2007. A component based noise correction method (CompCor) for BOLD and perfusion based fMRI. Neuroimage 37 (1), 90–101. https://doi.org/10.1016/j.neuroimage.2007.04.042.

Bernstein, M., Yovel, G., 2015. Two neural pathways of face processing: a critical evaluation of current models. Neurosci. Biobehav. Rev. 55, 536–546. https://doi.org/10.1016/j.neubiorev.2015.06.010.

Bracci, S., Op de Beeck, H.P., 2023. Understanding human object vision: a picture is worth a thousand representations. Annu. Rev. Psychol. 74 (1), 113–135. https://doi.org/10.1146/annurev-psych-032720-041031.

Clark, I.A., Maguire, E.A., 2023. Release of cognitive and multimodal MRI data including real-world tasks and hippocampal subfield segmentations. Sci. Data 10 (1), 540. https://doi.org/10.1038/s41597-023-02449-9.

Cutting, J.E., Brunick, K.L., Candan, A., 2012. Perceiving event dynamics and parsing Hollywood films. J. Exp. Psychol. Hum. Percept. Perform. 38 (6), 1476–1490. https://doi.org/10.1037/a0027737.

Dale, A.M., Fischl, B., Sereno, M.I., 1999. Cortical surface-based analysis I. Segmentation and surface reconstruction. Neuroimage 9 (2), 179–194. https://doi.org/10.1006/nimg.1998.0395.

Davies-Thompson, J., Andrews, T.J., 2012. Intra- and interhemispheric connectivity between face-selective regions in the human brain. J. Neurophysiol. 108 (11), 3087–3095. https://doi.org/10.1152/jn.01171.2011.

Dilks, D.D., Kamps, F.S., Persichetti, A.S., 2022. Three cortical scene systems and their development. Trends Cognit. Sci. 26 (2), 117–127. https://doi.org/10.1016/j.tics.2021.11.002.

Duchaine, B., Nakayama, K., 2006. The Cambridge face memory test: results for neurologically intact individuals and an investigation of its validity using inverted face stimuli and prosopagnosic participants. Neuropsychologia 44 (4), 576–585. https://doi.org/10.1016/j.neuropsychologia.2005.07.001.

Duchaine, B., Yovel, G., 2015. A revised neural framework for face processing. Ann. Rev. Vis. Sci. 1, 393–416. https://doi.org/10.1146/annurev-vision-082114-035518.

Epstein, R.A., Baker, C.I., 2019. Scene perception in the human brain. Ann. Rev. Vis. Sci. 5 (1), 373–397. https://doi.org/10.1146/annurev-vision-091718-014809.

Finn, E.S., 2021. Is it time to put rest to rest? Trends Cognit. Sci. 25 (12), 1021–1032. https://doi.org/10.1016/j.tics.2021.09.005.

Finn, E.S., Shen, X., Scheinost, D., Rosenberg, M.D., Huang, J., Chun, M.M., Papademetris, X., Constable, R.T., 2015. Functional connectome fingerprinting: identifying individuals using patterns of brain connectivity. Nat. Neurosci. 18 (11), 1664–1671. https://doi.org/10.1038/nn.4135.

Glasser, M.F., Sotiropoulos, S.N., Wilson, J.A., Coalson, T.S., Fischl, B., Andersson, J.L., Xu, J., Jbabdi, S., Webster, M., Polimeni, J.R., Van Essen, D.C., Jenkinson, M., 2013. The minimal preprocessing pipelines for the human connectome project. Neuroimage 80, 105–124. https://doi.org/10.1016/j.neuroimage.2013.04.127.

Greve, D.N., Fischl, B., 2009. Accurate and robust brain image alignment using boundary-based registration. Neuroimage 48 (1), 63–72. https://doi.org/10.1016/j.neuroimage.2009.06.060.

Gschwind, M., Pourtois, G., Schwartz, S., Van De Ville, D., Vuilleumier, P., 2012. White-matter connectivity between face-responsive regions in the human brain. Cerebr. Cortex 22 (7), 1564–1576. https://doi.org/10.1093/cercor/bhr226.

Hanke, M., Adelhöfer, N., Kottke, D., Iacovella, V., Sengupta, A., Kaule, F.R., Nigbur, R., Waite, A.Q., Baumgartner, F., Stadler, J., 2016. A studyforrest extension, simultaneous fMRI and eye gaze recordings during prolonged natural stimulation. Sci. Data 3 (1), 160092. https://doi.org/10.1038/sdata.2016.92.

Hanke, M., Baumgartner, F.J., Ibe, P., Kaule, F.R., Pollmann, S., Speck, O., Zinke, W., Stadler, J., 2014. A high-resolution 7-Tesla fMRI dataset from complex natural stimulation with an audio movie. Sci. Data 1 (1), 140003. https://doi.org/10.1038/sdata.2014.3.

Harel, A., Kravitz, D.J., Baker, C.I., 2014. Task context impacts visual object processing differentially across the cortex. In: Proceedings of the National Academy of Sciences, pp. E962–E971. https://doi.org/10.1073/pnas.1312567111.

Haxby, J.V., Hoffman, E.A., Gobbini, M.I., 2000. The distributed human neural system for face perception. Trends Cognit. Sci. 4 (6), 223–233. https://doi.org/10.1016/S1364-6613(00)01482-0.

Holm, S., 1979. A simple sequentially rejective multiple test procedure. Scand. J. Stat. 6 (2), 65–70.

Jenkinson, M., Bannister, P., Brady, M., Smith, S., 2002. Improved optimization for the robust and accurate linear registration and motion correction of brain images. Neuroimage 17 (2), 825–841. https://doi.org/10.1006/nimg.2002.1132.

Jenkinson, M., Beckmann, C.F., Behrens, T.E.J., Woolrich, M.W., Smith, S.M., 2012. FSL. Neuroimage 62 (2), 782–790. https://doi.org/10.1016/j.neuroimage.2011.09.015.

Julian, J.B., Keinath, A.T., Marchette, S.A., Epstein, R.A., 2018. The neurocognitive basis of spatial reorientation. Curr. Biol. 28 (17), R1059–R1073. https://doi.org/10.1016/j.cub.2018.04.057.

Kennedy, B., Malladi, S.N., Tootell, R.B., Nasr, S., 2024. A previously undescribed scene-selective site is the key to encoding ego-motion in naturalistic environments. eLife 13, RP91601. https://doi.org/10.7554/eLife.91601.

Kim, D., Kay, K., Shulman, G.L., Corbetta, M., 2018. A new modular brain organization of the BOLD signal during natural vision. Cerebr. Cortex 28 (9), 3065–3081. https://doi.org/10.1093/cercor/bhx175.

Kröll, J.-P., Friedrich, P., Li, X., Patil, K.R., Mochalski, L., Waite, L., Qian, X., Chee, M.W., Zhou, J.H., Eickhoff, S., Weis, S., 2023. Naturalistic viewing increases individual identifiability based on connectivity within functional brain networks. Neuroimage 273 (October 2022), 120083. https://doi.org/10.1016/j.neuroimage.2023.120083.

Kubota, E., Yan, X., Tung, S., Fascendini, B., Tyagi, C., Duhameau, S., Ortiz, D., Grotheer, M., Natu, V.S., Keil, B., Grill-Spector, K., 2025. White matter connections of human ventral temporal cortex are organized by cytoarchitecture, eccentricity and category-selectivity from birth. Nat. Hum. Behav. 9 (5), 955–970. https://doi.org/10.1038/s41562-025-02116-6.

Lakens, D., 2013. Calculating and reporting effect sizes to facilitate cumulative science: a practical primer for t-tests and ANOVAs. Front. Psychol. 4 (NOV), 1–12. https://doi.org/10.3389/fpsyg.2013.00863.

Langner, O., Dotsch, R., Bijlstra, G., Wigboldus, D.H.J., Hawk, S.T., van Knippenberg, A., 2010. Presentation and validation of the Radboud faces database. Cognit. Emot. 24 (8), 1377–1388. https://doi.org/10.1080/02699930903485076.

Lynch, L.K., Lu, K., Wen, H., Zhang, Y., Saykin, A.J., Liu, Z., 2018. Task-evoked functional connectivity does not explain functional connectivity differences between rest and task conditions. Hum. Brain Mapp. 39 (12), 4939–4948. https://doi.org/10.1002/hbm.24335.

Mars, R.B., Sotiropoulos, S.N., Passingham, R.E., Sallet, J., Verhagen, L., Khrapitchev, A.A., Sibson, N., Jbabdi, S., 2018. Whole brain comparative anatomy using connectivity blueprints. eLife 7, e35237. https://doi.org/10.7554/eLife.35237.

Molloy, M.F., Saygin, Z.M., Osher, D.E., 2024. Predicting high-level visual areas in the absence of task fMRI. Sci. Rep. 14 (1), 11376. https://doi.org/10.1038/s41598-024-62098-9.

Noad, K.N., Watson, D.M., Andrews, T.J., 2024. Familiarity enhances functional connectivity between visual and nonvisual regions of the brain during natural viewing. Cerebr. Cortex 34 (7). https://doi.org/10.1093/cercor/bhae285 bhae285.

Olejnik, S., Algina, J., 2003. Generalized eta and omega squared statistics: measures of effect size for some common research designs. Psychol. Methods 8 (4), 434–447. https://doi.org/10.1037/1082-989X.8.4.434.

Osher, D.E., Saxe, R.R., Koldewyn, K., Gabrieli, J.D.E., Kanwisher, N., Saygin, Z.M., 2016. Structural connectivity fingerprints predict cortical selectivity for multiple visual categories across cortex. Cerebr. Cortex 26 (4), 1668–1683. https://doi.org/10.1093/cercor/bhu303.

Passingham, R.E., Stephan, K.E., Kötter, R., 2002. The anatomical basis of functional localization in the cortex. Nat. Rev. Neurosci. 3 (8), 606–616. https://doi.org/10.1038/nrn893.

Peelen, M.V., Downing, P.E., 2017. Category selectivity in human visual cortex: beyond visual object recognition. Neuropsychologia 105 (March), 177–183. https://doi.org/10.1016/j.neuropsychologia.2017.03.033.

Peirce, J., Gray, J.R., Simpson, S., MacAskill, M., Höchenberger, R., Sogo, H., Kastman, E., Lindeløv, J.K., 2019. PsychoPy2: experiments in behavior made easy. Behav. Res. Methods 3. https://doi.org/10.3758/s13428-018-01193-y.

Pitcher, D., Ungerleider, L.G., 2021. Evidence for a third visual pathway specialized for social perception. Trends Cognit. Sci. 25 (2), 100–110. https://doi.org/10.1016/j.tics.2020.11.006.

Pruim, R.H.R., Mennes, M., van Rooij, D., Llera, A., Buitelaar, J.K., Beckmann, C.F., 2015. ICA-AROMA: a robust ICA-Based strategy for removing motion artifacts from fMRI data. Neuroimage 112, 267–277. https://doi.org/10.1016/j.neuroimage.2015.02.064.

Pyles, J.A., Verstynen, T.D., Schneider, W., Tarr, M.J., 2013. Explicating the face perception network with white matter connectivity. PLoS One 8 (4), e61611. https://doi.org/10.1371/journal.pone.0061611.

Raichle, M.E., 2015. The brain's default mode network. Annu. Rev. Neurosci. 38 (1), 433–447. https://doi.org/10.1146/annurev-neuro-071013-014030.

Rajimehr, R., Xu, H., Farahani, A., Kornblith, S., Duncan, J., Desimone, R., 2024. Functional architecture of cerebral cortex during naturalistic movie watching. Neuron 112 (24), 4130–4146.e3. https://doi.org/10.1016/j.neuron.2024.10.005.

Robinson, E.C., Garcia, K., Glasser, M.F., Chen, Z., Coalson, T.S., Makropoulos, A., Bozek, J., Wright, R., Schuh, A., Webster, M., Hutter, J., Price, A., Cordero Grande, L., Hughes, E., Tusor, N., Bayly, P.V., Van Essen, D.C., Smith, S.M., Edwards, A.D., et al., 2018. Multimodal surface matching with higher-order smoothness constraints. Neuroimage 167 (October 2017), 453–465. https://doi.org/10.1016/j.neuroimage.2017.10.037.

Robinson, E.C., Jbabdi, S., Glasser, M.F., Andersson, J., Burgess, G.C., Harms, M.P., Smith, S.M., Van Essen, D.C., Jenkinson, M., 2014. MSM: a new flexible framework for multimodal surface matching. Neuroimage 100, 414–426. https://doi.org/10.1016/j.neuroimage.2014.05.069.

Rosenberg, M.D., Finn, E.S., Scheinost, D., Papademetris, X., Shen, X., Constable, R.T., Chun, M.M., 2016. A neuromarker of sustained attention from whole-brain functional connectivity. Nat. Neurosci. 19 (1), 165–171. https://doi.org/10.1038/nn.4179.

Russell, R., Duchaine, B., Nakayama, K., 2009. Super-recognizers: people with extraordinary face recognition ability. Psychon. Bull. Rev. 16 (2), 252–257. https://doi.org/10.3758/PBR.16.2.252.

Salimi-Khorshidi, G., Douaud, G., Beckmann, C.F., Glasser, M.F., Griffanti, L., Smith, S.M., 2014. Automatic denoising of functional MRI data: combining independent component analysis and hierarchical fusion of classifiers. Neuroimage 90, 449–468. https://doi.org/10.1016/j.neuroimage.2013.11.046.

Saygin, Z.M., Osher, D.E., Koldewyn, K., Reynolds, G., Gabrieli, J.D.E., Saxe, R.R., 2012. Anatomical connectivity patterns predict face selectivity in the fusiform gyrus. Nat. Neurosci. 15 (2), 321–327. https://doi.org/10.1038/nn.3001.

Saygin, Z.M., Osher, D.E., Norton, E.S., Youssoufian, D.A., Beach, S.D., Feather, J., Gaab, N., Gabrieli, J.D.E., Kanwisher, N., 2016. Connectivity precedes function in the development of the visual word form area. Nat. Neurosci. 19 (9), 1250–1255. https://doi.org/10.1038/nn.4354.

Schaefer, A., Kong, R., Gordon, E.M., Laumann, T.O., Zuo, X.-N., Holmes, A.J., Eickhoff, S.B., Yeo, B.T.T., 2018. Local-global parcellation of the human cerebral cortex from intrinsic functional connectivity MRI. Cerebr. Cortex 28 (9), 3095–3114. https://doi.org/10.1093/cercor/bhx179.

Sengupta, A., Kaule, F.R., Guntupalli, J.S., Hoffmann, M.B., Häusler, C., Stadler, J., Hanke, M., 2016. A studyforrest extension, retinotopic mapping and localization of higher visual areas. Sci. Data 3 (1), 160093. https://doi.org/10.1038/sdata.2016.93.

Shen, X., Finn, E.S., Scheinost, D., Rosenberg, M.D., Chun, M.M., Papademetris, X., Constable, R.T., 2017. Using connectome-based predictive modeling to predict individual behavior from brain connectivity. Nat. Protoc. 12 (3), 506–518. https://doi.org/10.1038/nprot.2016.178.

Silson, E.H., Steel, A., Kidder, A., Gilmore, A.W., Baker, C.I., 2019. Distinct subdivisions of human medial parietal cortex support recollection of people and places. eLife 8, 554915. https://doi.org/10.7554/eLife.47391.

Smith, S.M., 2002. Fast robust automated brain extraction. Hum. Brain Mapp. 17 (3), 143–155. https://doi.org/10.1002/hbm.10062.

Smith, S.M., Beckmann, C.F., Andersson, J., Auerbach, E.J., Bijsterbosch, J., Douaud, G., Duff, E., Feinberg, D.A., Griffanti, L., Harms, M.P., Kelly, M., Laumann, T., Miller, K.L., Moeller, S., Petersen, S., Power, J., Salimi-Khorshidi, G., Snyder, A.Z., Vu, A.T., et al., 2013. Resting-state fMRI in the human connectome project. Neuroimage 80, 144–168. https://doi.org/10.1016/j.neuroimage.2013.05.039.

Steel, A., Billings, M.M., Silson, E.H., Robertson, C.E., 2021. A network linking scene perception and spatial memory systems in posterior cerebral cortex. Nat. Commun. 12 (1), 2632. https://doi.org/10.1038/s41467-021-22848-z.

Van Essen, D.C., Glasser, M.F., Dierker, D.L., Harwell, J., Coalson, T., 2012a. Parcellations and hemispheric asymmetries of human cerebral cortex analyzed on surface-based atlases. Cerebr. Cortex 22 (10), 2241–2262. https://doi.org/10.1093/cercor/bhr291.

Van Essen, D.C., Ugurbil, K., Auerbach, E., Barch, D., Behrens, T.E.J., Bucholz, R., Chang, A., Chen, L., Corbetta, M., Curtiss, S.W., Della Penna, S., Feinberg, D., Glasser, M.F., Harel, N., Heath, A.C., Larson-Prior, L., Marcus, D., Michalareas, G., Moeller, S., et al., 2012b. The human connectome project: a data acquisition perspective. Neuroimage 62 (4), 2222–2231. https://doi.org/10.1016/j.neuroimage.2012.02.018.

Wang, G., Foxwell, M.J., Cichy, R.M., Pitcher, D., Kaiser, D., 2024. Individual differences in internal models explain idiosyncrasies in scene perception. Cognition 245 (January), 105723. https://doi.org/10.1016/j.cognition.2024.105723.

Watson, D.M., Andrews, T.J., 2024. Mapping the functional and structural connectivity of the scene network. Hum. Brain Mapp. 45 (3), e26628. https://doi.org/10.1002/hbm.26628.

White, D., Burton, A.M., 2022. Individual differences and the multidimensional nature of face perception. Nat. Rev. Psychol. 1 (5), 287–300. https://doi.org/10.1038/s44159-022-00041-3.

Woolrich, M.W., Behrens, T.E.J., Beckmann, C.F., Jenkinson, M., Smith, S.M., 2004. Multilevel linear modelling for FMRI group analysis using Bayesian inference. Neuroimage 21 (4), 1732–1747. https://doi.org/10.1016/j.neuroimage.2003.12.023.

Woolrich, M.W., Ripley, B.D., Brady, M., Smith, S.M., 2001. Temporal autocorrelation in univariate linear modeling of FMRI data. Neuroimage 14 (6), 1370–1386. https://doi.org/10.1006/nimg.2001.0931.

Xiao, J.X., Hays, J., Ehinger, K.A., Oliva, A., Torralba, A., 2010. SUN database: large-scale scene recognition from abbey to zoo. In: IEEE Conference on Computer Vision and Pattern Recognition, pp. 3485–3492. https://doi.org/10.1109/cvpr.2010.5539970.

Yeo, B.T., Krienen, F.M., Sepulcre, J., Sabuncu, M.R., Lashkari, D., Hollinshead, M., Roffman, J.L., Smoller, J.W., Zöllei, L., Polimeni, J.R., Fischl, B., Liu, H., Buckner, R.L., 2011. The organization of the human cerebral cortex estimated by intrinsic functional connectivity. J. Neurophysiol. 106 (3), 1125–1165. https://doi.org/10.1152/jn.00338.2011.

Yoon, H.K., Jung, Y., Persichetti, A.S., Dilks, D.D., 2025. A scene-selective region in the superior parietal lobule for visually guided navigation. Cerebr. Cortex 35 (4). https://doi.org/10.1093/cercor/bhaf082.

Zhang, Y., Brady, M., Smith, S., 2001. Segmentation of brain MR images through a hidden markov random field model and the expectation-maximization algorithm. IEEE Trans. Med. Imag. 20 (1), 45–57. https://doi.org/10.1109/42.906424.

Zhi, D., King, M., Hernandez-Castillo, C.R., Diedrichsen, J., 2022. Evaluating brain parcellations using the distance-controlled boundary coefficient. Hum. Brain Mapp. 1–15. https://doi.org/10.1002/hbm.25878. October 2021.